



One- and two-dimensional solitons under the action of the inverted cubic-quintic nonlinearity



Liangwei Zeng ^{1,2}, Boris A. Malomed ^{3,4}, Dumitru Mihalache ⁵ & Xing Zhu ¹

The usual cubic-quintic (CQ) nonlinearity is proved to sustain one- and two-dimensional (1D and 2D) broad (flat-top) solitons. In this work, we demonstrate that 1D and 2D soliton families can be supported, in the semi-infinite bandgap (SIBG), by the interplay of a lattice potential and the nonlinearity including self-defocusing cubic and self-focusing quintic terms, with the sign combination inverted with respect to the usual CQ nonlinearity. The families include fundamental and dipole solitons in 1D, and fundamental, quadrupole, and vortex solitons in 2D. The power, shapes, and stability of the solitons are reported. The results are strongly affected by the positions of the solitons in SIBG, the families being unstable very close to or very far from the SIBG's edge. The inverted CQ nonlinearity, considered in this work, sustains sharp 1D and 2D stable solitons, which can be naturally used as bit pixels in photonic data-processing applications.

The formation of solitons^{1–3} is a fundamental topic in nonlinear physics^{4–8}, especially in the fields of nonlinear optics and photonics^{9–15} and quantum matter, such as Bose-Einstein condensates (BECs)^{16–22}. Various types of soliton families have been reported, a majority of them representing one-dimensional (1D) states^{23–25}. The creation of 2D solitons is a challenging issue, as self-focusing cubic and quintic nonlinear terms acting in the free 2D space, modeled by equations of the nonlinear-Schrödinger (NLS) type, give rise to the critical and supercritical collapse, respectively, which makes all free-space solitons, supported by the self-focusing, unstable in 2D^{26–29}. To stabilize 2D and 3D solitons against the collapse, it was proposed to use linear and nonlinear potentials^{29–33}. In particular, spatially periodic linear and nonlinear potentials, alias linear^{30,31,34–36} and nonlinear^{37–41} lattices, can be used to build various types of stable 2D solitons, including fundamental ones⁴², dipoles^{43–45}, multipoles^{46,47}, solitary vortices^{48,49}, and half-vortices⁵⁰. The stable 2D solitons, pinned to the underlying lattice, offer a significant potential for the use as bit pixels in various data-processing schemes^{51,52}. Obviously, narrow 2D solitons are required to realize this application.

Another setting that provides stabilization of 2D^{53–56} and 3D^{57,58} solitons, including ones with embedded vorticity, includes competition of the self-focusing cubic and defocusing quintic nonlinear terms, which can be readily implemented in optical waveguides. In particular, stable 2D^{53,54} and 3D⁵⁷ vortex solitons, as well as the fundamental (zero-vorticity) ones⁵⁹, supported by the cubic-quintic (CQ) nonlinearity have been predicted. A characteristic feature of these modes is their flat-top shape, as the increase of

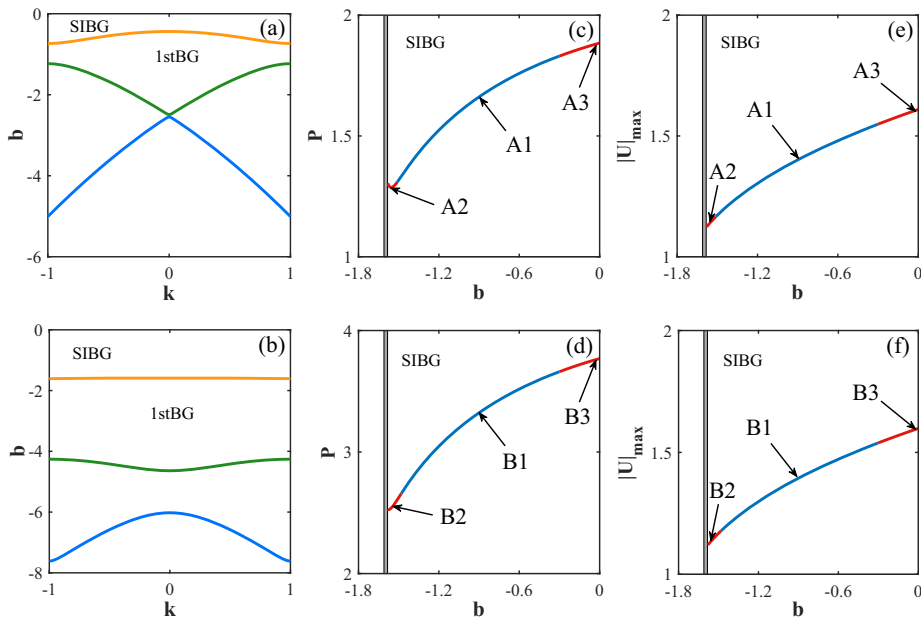
the input optical power can be accommodated by the spatial expansion of the solitons, while their local intensity is bounded by the balance of the cubic self-focusing and quintic self-defocusing nonlinearities.

While the composite nonlinearity of this type is quite natural, as it appears as an approximate form of the saturable nonlinear response of the dielectric medium to the propagating electromagnetic waves, other types are physically relevant too. As demonstrated experimentally and explained theoretically^{60–62}, the CQ nonlinearity (and its extension including the septimal term)^{63,64} can be efficiently engineered, including a possibility to separately choose the signs and magnitudes of the cubic and quintic terms, in optical materials based on colloidal suspensions of metallic nanoparticles, using their radius, which takes values in the range of 1–100 nm, and volume fraction f of the nanoparticles, varying in the range of 10^{-5} – 10^{-4} , as control parameters. The effective nonlinearity is produced by the nanoparticles through the surface-plasmon-resonance mechanism.

The freedom in the engineering of the composite nonlinearities suggests one to consider the “unusual” case of the *inverted* CQ nonlinearity, composed of defocusing cubic and focusing quintic terms, which is the subject of the present work. The inverted CQ nonlinearity should be considered in the combination with a lattice potential, as, otherwise, there is no chance to construct any stable self-trapped state in the model. In this work, we demonstrate that this setting is promising for the above-mentioned applications, as the stable solitons can be maintained by the interplay of the cubic self-defocusing and quintic self-focusing nonlinearities in the desired

¹School of Arts and Sciences, Guangzhou Maritime University, Guangzhou, China. ²College of Physics and Optoelectronic Engineering, Shenzhen University, Shenzhen, China. ³Department of Physical Electronics, School of Electrical Engineering, Faculty of Engineering, and Center for Light-Matter Interaction, Tel Aviv University, Tel Aviv, Israel. ⁴Instituto de Alta Investigación, Universidad de Tarapacá, Arica, Chile. ⁵Horia Hulubei National Institute of Physics and Nuclear Engineering, Magurele, Bucharest, Romania. e-mail: xingzhu@gzmtu.edu.cn

Fig. 1 | Bandgap spectra, power and amplitude of 1D soliton families. **a, b** The bandgap spectrum produced by the 1D version of the linearized equation (5) with potential (3), for $V_0 = 1$ (a) and $V_0 = 6$ (b). The spectrum is plotted in the plane of the quasi-momentum k of Bloch modes and propagation constant b . The red, blue, and green strips represent the first, second, and third Bloch bands, respectively. Acronyms SIBG and 1stBG stand for the semi-infinite and first bandgaps, respectively. **c, d** The soliton's power P vs. propagation constant b in the SIBG for families of 1D fundamental (c) and dipole (d) solitons in the deep lattice potential, with $V_0 = 6$. Blue and red segments of the curves represent stable and unstable solitons, respectively. **e, f** The amplitude (maximum value of $|U(x)|$) of the families of 1D fundamental (e) and dipole (f) solitons at $V_0 = 6$. The vertical gray areas in panels (c–f) stand for the first Bloch band.



form of narrow pixels, while the usual combination of the cubic focusing and quintic defocusing nonlinearities gives rise to the above-mentioned broad (flat-top) modes, which cannot be used as pixels.

It is relevant to mention that, in the case of the cubic or quintic self-defocusing per se, self-trapped modes can be found as gap solitons populating finite bandgaps induced by the lattice potential, while no bright solitons exist in the semi-infinite bandgap (SIBG)⁶⁵. In the case of the self-focusing nonlinearity, solitons populate the SIBG, but do not exist in finite bandgaps. In the latter case, 2D solitons are unstable in the free-space SIBG (no lattice potential) due to the occurrence of the collapse^{26–29}. Nevertheless, both fundamental and vortical 2D solitons can be readily stabilized in the SIBG by the lattice potential in the self-focusing cubic medium^{30,31}. The objective of the present work is to produce families of stable 1D and 2D bright solitons in SIBG under the combined action of the lattice potential and *inverted* CQ nonlinearity. These are narrow (pixel-like) solitons of the fundamental and dipole types in 1D, and ones of the fundamental, quadrupole, and vortex types in 2D. The soliton solutions are constructed in the numerical form, and their stability is identified by means of systematically performed simulations of the perturbed propagation. We conclude that the position of the solitons in the SIBG essentially affects their shape and stability.

The subsequent presentation is arranged as follows. Systematically collected numerical results for the soliton families are presented in the section of results, which is divided in two parts, reporting the findings for 1D and 2D solitons. The paper is concluded by the section of conclusion. Then the model is introduced in section of “Methods”, where we also produce some simple analytical results for broad and narrow solitons, which suggest their stability in terms of the well-known Vakhitov-Kolokolov (VK) criterion^{26,66}.

Results

One-dimensional solitons

The Bloch bandgap structure^{67,68} produced by the linearization of the 1D version of Eq. (5) with lattice potential (3) is plotted in Fig. 1a, b, for the moderate ($V_0 = 1$) and deep ($V_0 = 6$) potentials, respectively, with SIBG and 1stBG standing for the semi-infinite bandgap and the first finite bandgap, respectively, which are separated by thin Bloch bands plotted by curves of different colors.

It is observed that solely the first finite bandgap is open at $V_0 = 1$, while there are two of them at $V_0 = 6$. Here we address 1D solitons in SIBG. The family of the fundamental solitons is represented in Fig. 1c by the respective

dependence of the soliton's power P (see Eq. (7)) on propagation constant b . The $P(b)$ features a narrow VK-unstable interval with $dP/db < 0$, followed by a broad one with $dP/db > 0$. In addition, a family of 1D dipole solitons is represented by the corresponding $P(b)$ curve in Fig. 1d. Naturally, for any given b , the power of the dipoles is approximately twice its counterparts for the fundamental solitons plotted in Fig. 1c.

Blue and red segments of the curves displayed in Fig. 1c, d represent stable and unstable parts of the respective soliton families. Obviously, all stable subfamilies satisfy the VK criterion, $dP/db > 0$, which, as said above, is a necessary (but not sufficient) condition for the stability of solitons^{26,66}. The transition to instability of the fundamental and dipole solitons at larger values of the power (at $P > 1.83$ and $P > 3.66$, respectively, which correspond, approximately, to $-b < 0.3$), i.e., deeper in the SIBG, is a natural effect, as, deeply enough, the effect of the lattice potential becomes immaterial, and the combination of the defocusing cubic and focusing quintic nonlinear terms leads to instability as usual.

Profiles of typical 1D fundamental and dipole solitons, which are marked by labels A1, A2 and B1, B2 in Fig. 1c, d are plotted in Fig. 2. It is observed that, in accordance with the above-mentioned expectation, the solitons take the shape of narrow pixels, which makes them appropriate for applications. Further, note that each peak of $|U(x)|$ of the stable dipole, plotted at $b = -0.9$ in Fig. 2b, is similar to the stable fundamental soliton, which is plotted in Fig. 2a for the same value of b . While the stable solitons, such the fundamental and dipole ones, displayed here for $b = -0.9$, which reside deep in the SIBG, feature, respectively, the simple single- or double-peak shapes, unstable solitons, which reside close to the SIBG edge (such as the ones displayed in Fig. 2d, e for $b = -1.55$), demonstrate additional lower peaks near the main ones, which makes their shape essentially different from that of pixels. This feature is naturally explained by the fact that the unstable solitons are located close to the Bloch modes, which are represented by spatially periodic multi-peak patterns. The eigenvalues λ , produced by the numerical solution of Eq. (10) for the solitons in panels (b) and (e), are presented in panels (c) and (f), respectively. Obviously, panel (c) implies that the soliton in panel (b) is stable, while the one in panel (e) is unstable, according to panel (f).

To further investigate the variation of the solitons with the decrease of $|b|$ for the 1D solitons, we display their amplitude $|U(x)|_{\max}$ vs. the propagation constant b for 1D fundamental and dipole gap solitons in Fig. 1e, f, respectively. It is obvious that the amplitude grows monotonously with the decrease of $|b|$, being nearly identical for the fundamental solitons and dipoles.

Fig. 2 | Profiles and eigenvalues of linear stability analysis for 1D soliton families. Profiles of the 1D stable fundamental (a) and dipole (b) soliton found at $b = -0.9$, which correspond, respectively, to labels A1 and B1 in Fig. 1c, d. c Eigenvalues produced by the numerical solution of Eq. (10) for the soliton in (b). Unstable fundamental and dipole solitons, found at $b = -1.55$, which correspond to labels A2 and B2 in Fig. 1c, d, are plotted in panels (d) and (e), respectively. f Eigenvalues λ produced by Eq. (10) for the soliton in panel (e). The corresponding solutions of Eq. (5) are obtained for potential (3) with $V_0 = 6$.

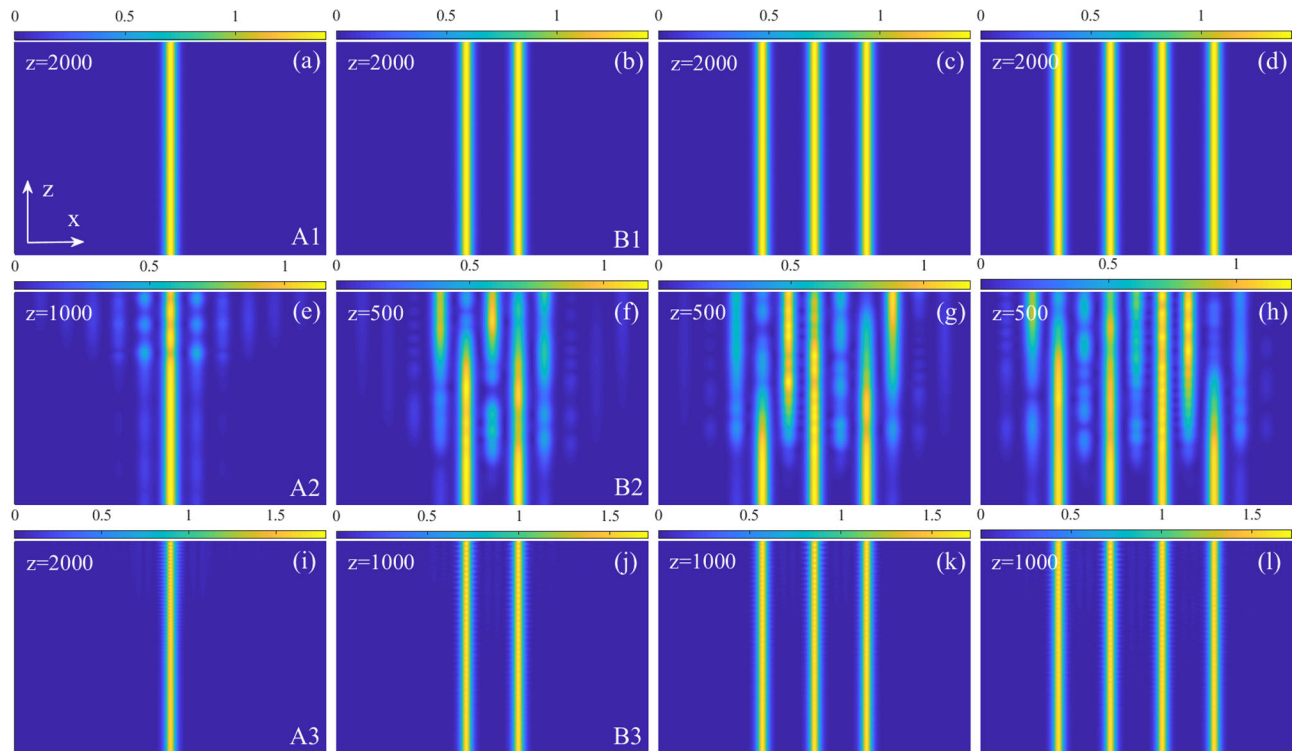
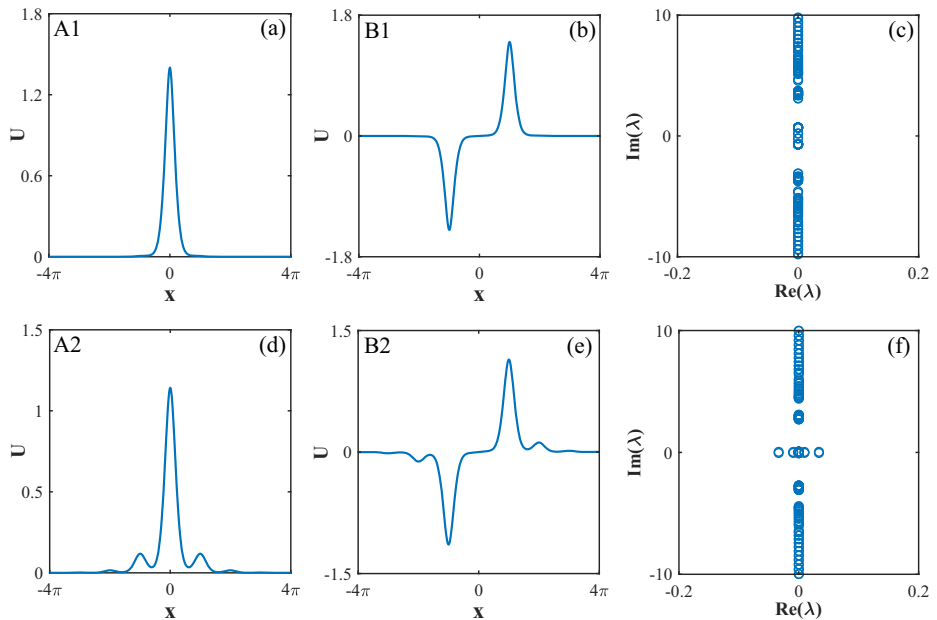


Fig. 3 | Perturbed propagations of 1D soliton families. The top row displays the stable perturbed propagation of 1D solitons with $b = -0.9$: a the fundamental soliton (which corresponds to point A1 in Fig. 1c); b the dipole soliton (corresponding to point B1 in Fig. 1d); c the tripole soliton; d the quadrupole one. The middle row displays the unstable propagation of the solitons with $b = -1.55$: e the fundamental

soliton (corresponding to point A2 in Fig. 1c); f the dipole soliton (corresponding to point B2 in Fig. 1d); g the tripole soliton; h the quadrupole one. The bottom row displays the unstable propagation of the solitons with $b = -0.02$: i the fundamental soliton (corresponding to point A3 in Fig. 1c); j the dipole soliton (corresponding to point B3 in Fig. 1d); k the tripole soliton; l the quadrupole one.

The (in)stability of the 1D solitons, which are represented by the blue (stable) and red (unstable) colors of the $P(b)$ curves in Fig. 1c, d, was corroborated by simulations of the perturbed evolution, examples of which are presented in Fig. 3, including the evolution of the solitons whose stationary shape is displayed in Fig. 2, which correspond to $b = -0.9$ and $b = -1.55$ for stable and unstable ones, respectively. In particular, in this and other cases, the unstable solitons exhibit gradual decay in the course of the propagation.

In addition to the fundamental and dipole solitons, Fig. 3 also exhibits examples of stable and unstable higher-order solitons, *viz.*, tripole and quadrupole ones, which can be readily constructed as additional solutions of Eq. (5). As well as the fundamental and dipole solitons, the higher-order ones are stable for $b = -0.9$ and unstable for $b = -1.55$.

The evolution of unstable fundamental and dipole solitons, which belong to the red high-power segments in Fig. 1c, d, is displayed in panels (a)

Fig. 4 | The 2D Bandgap spectra. **a, b** The bandgap spectrum produced by the linear version of the 2D equation (5) with potential (2), for $V_0 = 1$ (a) and $V_0 = 6$ (b). The spectrum shows the propagation constant b of Bloch modes vs. the components k_x and k_y of their quasi-momentum. As in Fig. 1, acronyms SIBG and 1stBG stand for the semi-infinite and the first bandgaps, respectively. In (a), surfaces denote, from top to bottom, the first, second, third, fourth, and fifth Bloch bands.

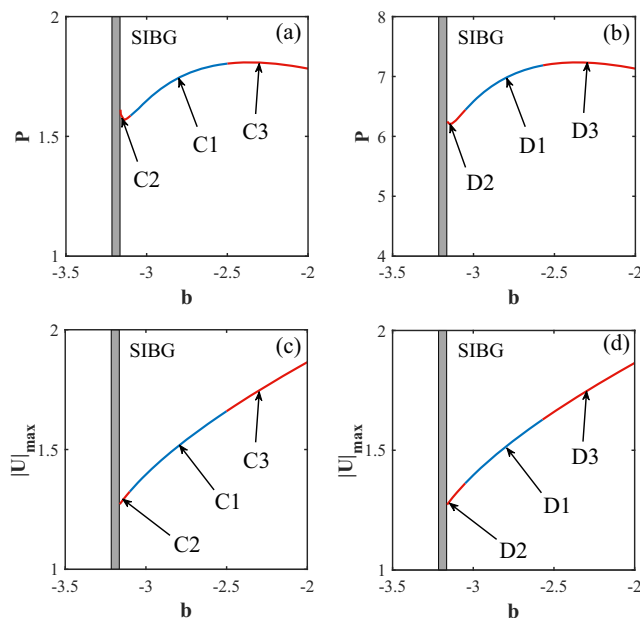
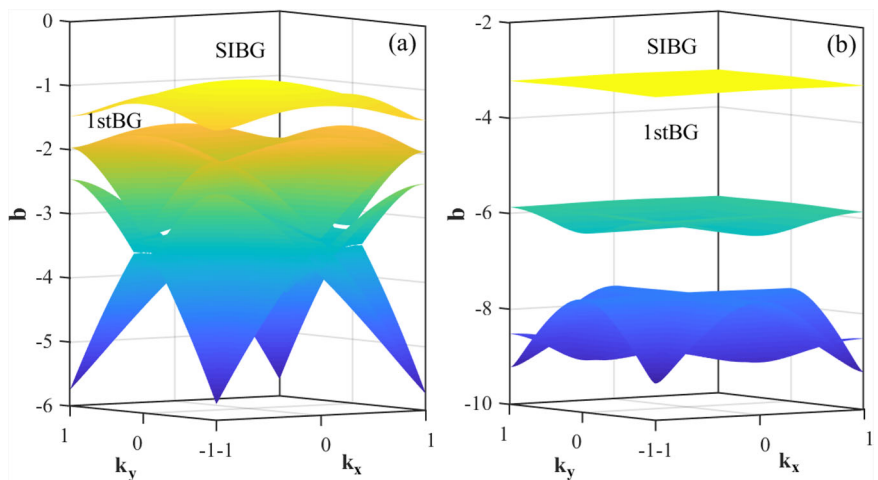


Fig. 5 | Power and amplitude of 2D soliton families. The curves of the soliton power P versus the propagation constant b in the semi-infinite bandgap of the 2D soliton families at $V_0 = 6$: **a** for the fundamental solitons; **b** for the quadrupoles. The amplitude (maximum value of $|U(x, y)|$) of the 2D soliton families at $V_0 = 6$: **c** for the fundamental solitons; **d** for the quadrupoles. The vertical gray areas in panels (a-d) stand for the first Bloch band.

and (j) of Fig. 3. The higher-order unstable solitons with high power are presented there too, featuring weak oscillations in the course of the evolution.

Two-dimensional solitons

The Bloch bandgap spectrum^{69–71} produced by the linearized version of the 2D equation (5) is presented in Fig. 4 for the 2D potential (2) with $V_0 = 1$ and $V_0 = 6$. As in Fig. 1, SIBG and 1stBG denote the semi-infinite and first finite bandgaps, respectively. Panel (a) shows that only a narrow first bandgap opens with $V_0 = 1$, while both the first and second ones open with $V_0 = 6$ in panel (b). As above, we here focus on solitons populating SIBG.

Families of 2D fundamental and quadrupole solitons, produced by the numerical solution of Eq. (5), are represented by the corresponding $P(b)$ curves (for the 2D integral power defined as per Eq. (6)) in Fig. 5a, b, where, similar to Fig. 1c, d, stable and unstable subfamilies are designated by the

blue and red colors, respectively. Naturally, for any given b the total power (6) of the quadrupole soliton is almost exactly fourfold the power of the fundamental soliton with the same b . A difference from the similar results for families of fundamental and dipole solitons in 1D, presented above in Fig. 1c, d, is that the transition to the instability deep inside SIBG is more pronounced (which is natural in the 2D case) and is explicitly related to the breakup of the VK criterion.

Similar to the situation reported for the 1D solitons in Fig. 1c, d, stable subfamilies of the 2D solitons obey the VK criterion in Fig. 5a, b. On the other hand, an essential difference from the results for the 1D model is that the $P(b)$ curves for the 2D solitons include relatively broad unstable segments deeper inside SIBG (specifically, these are ones at $-b < 2.5$ for the fundamental solitons, and at $-b < 2.57$ for quadrupoles), whose instability (unlike that of the above-mentioned narrow intervals of 1D unstable solitons in Fig. 1c, d, at $-b < 0.3$) is directly explained by the violation of the VK criterion. Indeed, the strongly destabilizing effect of the quintic self-focusing term deeply in SIBG, where the effect of the lattice potential is immaterial, is a natural feature in the 2D setting.

The families of the 2D fundamental and quadrupole solitons are additionally characterized, in Fig. 5c, d, by the respective dependences of their amplitude, $|U|_{\max}$, on the propagation constant b . These dependences, which are nearly identical for the fundamental solitons and quadrupoles, are quite similar to their counterparts for the 1D fundamental and dipole solitons, cf. Fig. 1e, f.

The shapes of the 2D fundamental solitons and quadrupoles, labeled by C1, C2 and D1, D2 in Fig. 5a, b, are plotted in Figs. 6 and 7, respectively, by means of 3D views and power contour plots in the (x, y) plane. Similar to what is reported above for the 1D solitons in Fig. 2, the stable 2D solitons and quadrupoles, located relatively deep in SIBG, feature isolated sharp peaks (a single one for the fundamental soliton, and four identical ones for the quadrupole), thus corroborating their potential use as pixels in the applications, while the unstable solitons and quadrupoles, residing close to the SIBG edge, exhibit additional small peaks around the major ones, which makes them different from pixels. The eigenvalues λ of the instability growth rate for these 2D modes are displayed in the right columns of Figs. 6 and 7. In addition, the perturbed propagation of the fundamental and quadrupole solitons are displayed in Figs. 8 and 9, respectively.

The stability of 2D solitons was also identified by means of systematic numerical simulations of their perturbed propagation. Typical examples of the stable and unstable propagation of the 2D fundamental soliton with propagation constants $b = -2.8$ and -3.15 are displayed in the left and middle columns of Fig. 8. In particular, the unstable mode suffers gradual decay in the course of the propagation, similar to the instability of the 1D solitons (cf. Fig. 3e–h). In addition, the unstable propagation of 2D

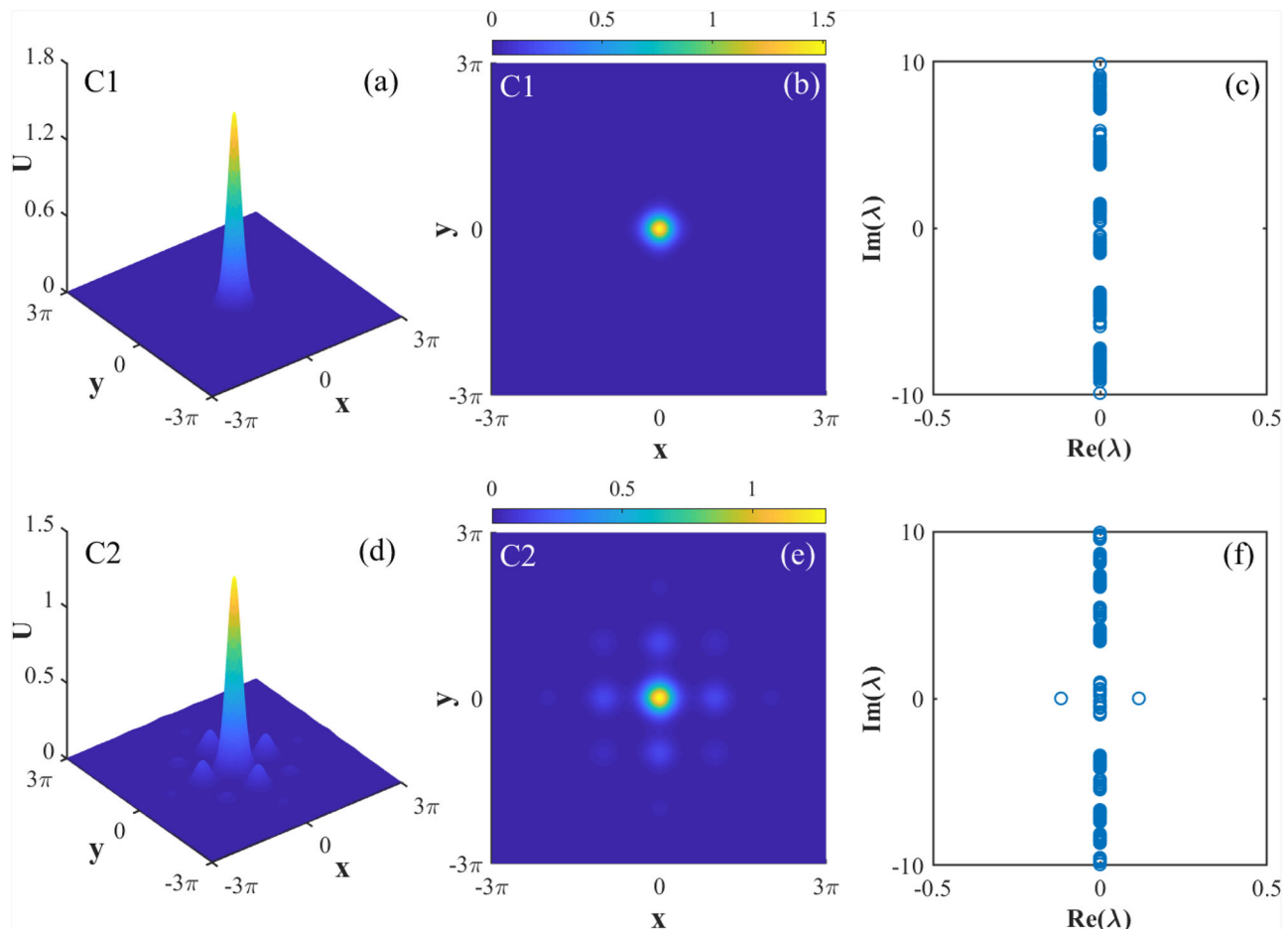


Fig. 6 | The 3D views, contour maps, and eigenvalues of linear stability analysis for 2D fundamental solitons. The 3D view (a), contour map of $|U(x, y)|$ (b), and eigenvalues λ produced by Eq. (10) (c) for the stable 2D fundamental soliton, labeled

C1 in Fig. 5a, which is obtained as the numerical solution of Eq. (5) with $b = -2.8$ and depth $V_0 = 6$ of the lattice potential (2). Panels (d–f) show the same, but for the unstable soliton with $b = -3.15$, which is labeled C2 in Fig. 5a.

fundamental solitons deep in SIBG (with $b = -2.3$) is displayed in the right column of Fig. 8. It is seen that the latter soliton suffers distortion in the course of the propagation.

Similar results for the perturbed propagation of stable and unstable quadrupole solitons are presented in Fig. 9. The gradual decay of unstable quadrupoles is similar to that exhibited by the unstable 2D fundamental solitons.

Solitons with embedded vorticity are also supported in the present model, as shown in Fig. 10 by means of the contour and phases plots, and the (in)stability eigenvalues for the vortex solitons with $b = -2.8$ and -3.1 . According to panel (c), the vortex from panel (a) is stable. On the other hand, the vortex soliton in panel (d) is unstable, according to (f).

The perturbed propagations of the vortex solitons from Fig. 10 is displayed in Fig. 11. This figure corroborates their stability in panels (a1, a2) and instability in (b1, b2), respectively. It is seen that the stable vortex soliton keeps its integrity in the course of the long-distance propagation (the top row), while the unstable one is destructed (the bottom row).

Conclusion

We have demonstrated that stable 1D and 2D solitons of several types (fundamental solitons, dipoles, quadrupoles, and vortices), belonging to the SIBG (semi-infinite bandgap) in the system's spectrum, can be sustained by the unusual (*inverted*) but physically relevant combination of the self-defocusing cubic and focusing quintic nonlinearities, in the combination with the lattice potentials. On the contrary to the broad (flat-top) solitons supported by the usual CQ (cubic-quintic)

nonlinearity, the inverted setting gives rise to stable narrow 1D and 2D ones, which may be used as bit pixels in photonic data-processing schemes. The inverted form of the CQ nonlinearity can be realized experimentally in terms of the light propagation in a colloidal material containing metallic nanoparticles. The soliton modes produced in this work are characterized by their shape, power, and stability, which are essentially affected by the position of the solitons in SIBG (semi-infinite bandgap). Stable 1D and 2D soliton families obey the well-known VK (Vakhitov-Kolokolov) stability criterion, the solitons being unstable in narrow intervals of the propagation constant near the SIBG's edge. Unlike the sharp (pixel-like) stable solitons, the unstable ones feature profiles that include low-amplitude peaks in addition to the sharp central ones. The solitons are also unstable deep inside SIBG, where the effect of the lattice potential becomes immaterial, and the combination of the defocusing cubic and focusing quintic terms naturally leads to the instability.

The model considered in this work may be realized in optical media. In particular, a natural implementation of the 1D and 2D settings is possible, respectively, in planar and bulk waveguides built in colloidal suspensions of metallic nanoparticles^{60–62}. The effective lattice potentials can be induced by spatially patterned distributions of dopants in the waveguide, which affect the linear interaction of the propagating light with the underlying material, cf. ref. 72.

The results reported in this work are helpful for the comprehensive understanding of the bright solitons supported by competing nonlinearities, such as that represented by the CQ terms with the inverted

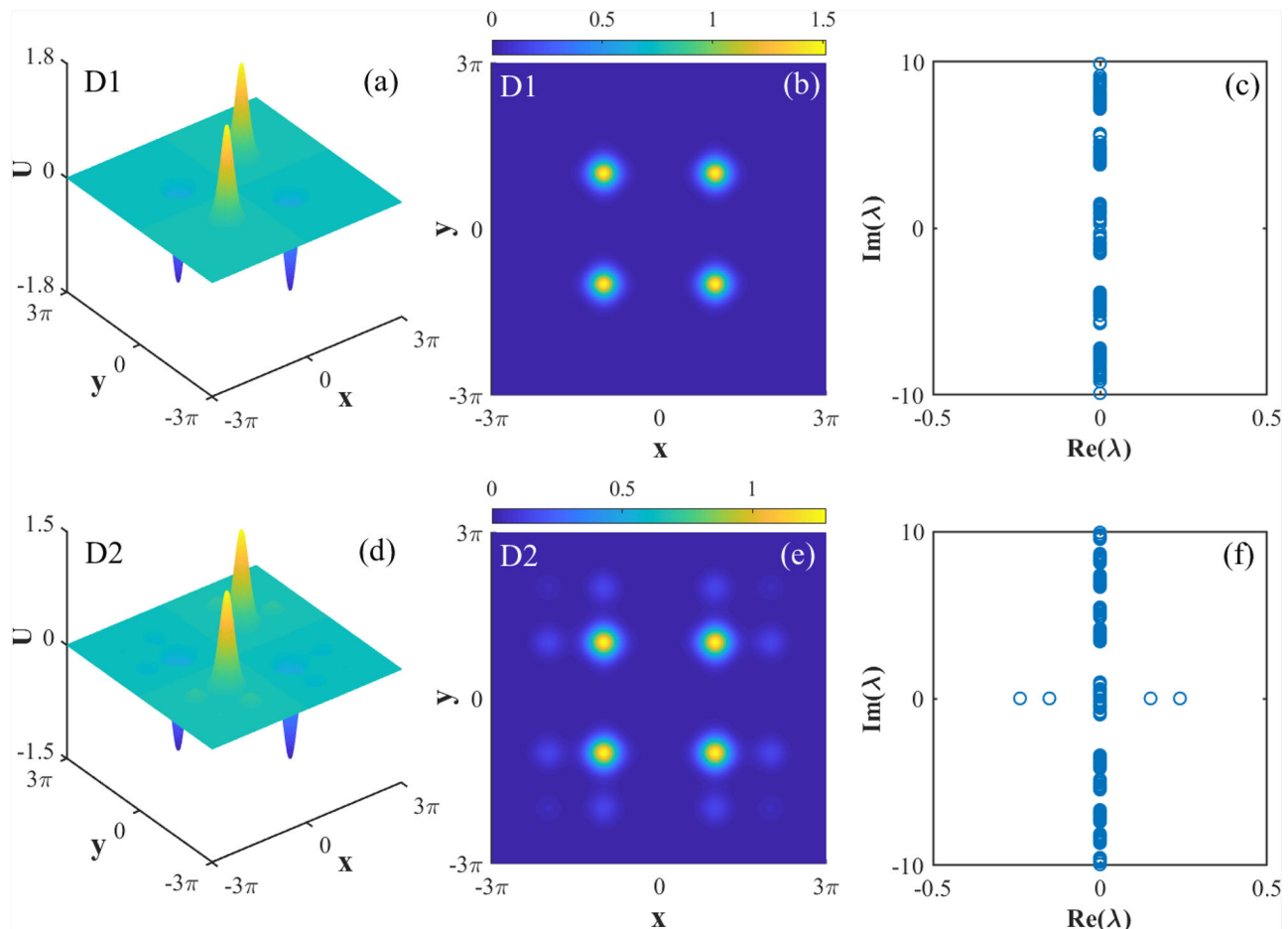


Fig. 7 | The 3D views, contour maps, and eigenvalues of linear stability analysis for 2D quadrupole solitons. The 3D view (a), contour map of $|U(x, y)|$ (b), and eigenvalues λ produced by Eq. (10) (c) for the stable 2D quadrupole soliton, labeled

D1 in Fig. 5b, which is obtained as the numerical solution of Eq. (5) with $b = -2.8$ and depth $V_0 = 6$ of the lattice potential (2). Panels (d–f) show the same, but for the unstable soliton with $b = -3.15$, which is labeled D2 in Fig. 5b.

combination of their signs (defocusing cubic and focusing quintic). The solitons of the fundamental and higher-order types (dipoles, multipoles, and vortices) are considered in the 1D and 2D geometries. The stable solitons, featuring narrow shapes, may find applications as pixels in photonic setups.

As an extension of the work, it may be interesting to explore vortex solitons with higher values of the topological charge, and 2D solitons in the model combining the inverted CQ nonlinearity in combination with lattice potentials of other types, such as triangular, hexagonal, and quasiperiodic. In addition, soliton families in two-component systems with the inverted CQ nonlinearity may also be an interesting subject, including the fundamental, dipole, multipole, and vortex solitons.

Methods

The basic equations

The propagation of amplitude $E(x, y; z)$ of the optical wave under the action of the inverted CQ nonlinearity, with the cubic and quintic coefficients, $g > 0$ and $\xi < 0$, and 2D lattice potential $V(x, y)$, is governed by the respective NLS equation, written in the scaled form^{56,73}:

$$i \frac{\partial E}{\partial z} = -\frac{1}{2} \nabla^2 E + V(x, y) E + g|E|^2 E + \xi|E|^4 E \quad (1)$$

(or its 1D reduction). Here, z is the propagation distance, and the paraxial-diffraction operator, $\nabla^2 = \partial^2/\partial x^2 + \partial^2/\partial y^2$, acts on the transverse coordinates, (x, y) . The lattice potentials with depth $2V_0 > 0$ (or $V_0 > 0$, in 1D) are taken

in the usual form⁶⁹,

$$V_{2D} = V_0 (\sin^2 x + \sin^2 y), \quad (2)$$

$$V_{1D} = V_0 \sin^2 x. \quad (3)$$

The numerical results are reported below for coefficients $g = 1$ and $\xi = -1$ (one of these values is fixed by scaling, while the choice of the other one makes it possible to produce generic results).

Stationary solutions of Eq. (1) with a real propagation constant b are looked for as

$$E = U(x, y) \exp(ibz), \quad (4)$$

where the stationary wave function U satisfies the equation

$$-bU = -\frac{1}{2} \nabla^2 U + V(x, y) U + g|U|^2 U + \xi|U|^4 U. \quad (5)$$

The 2D and 1D stationary solutions are characterized by their total power:

$$P_{2D} = \iint |U(x, y)|^2 dx dy, \quad (6)$$

$$P_{1D} = \int |U(x)|^2 dx. \quad (7)$$

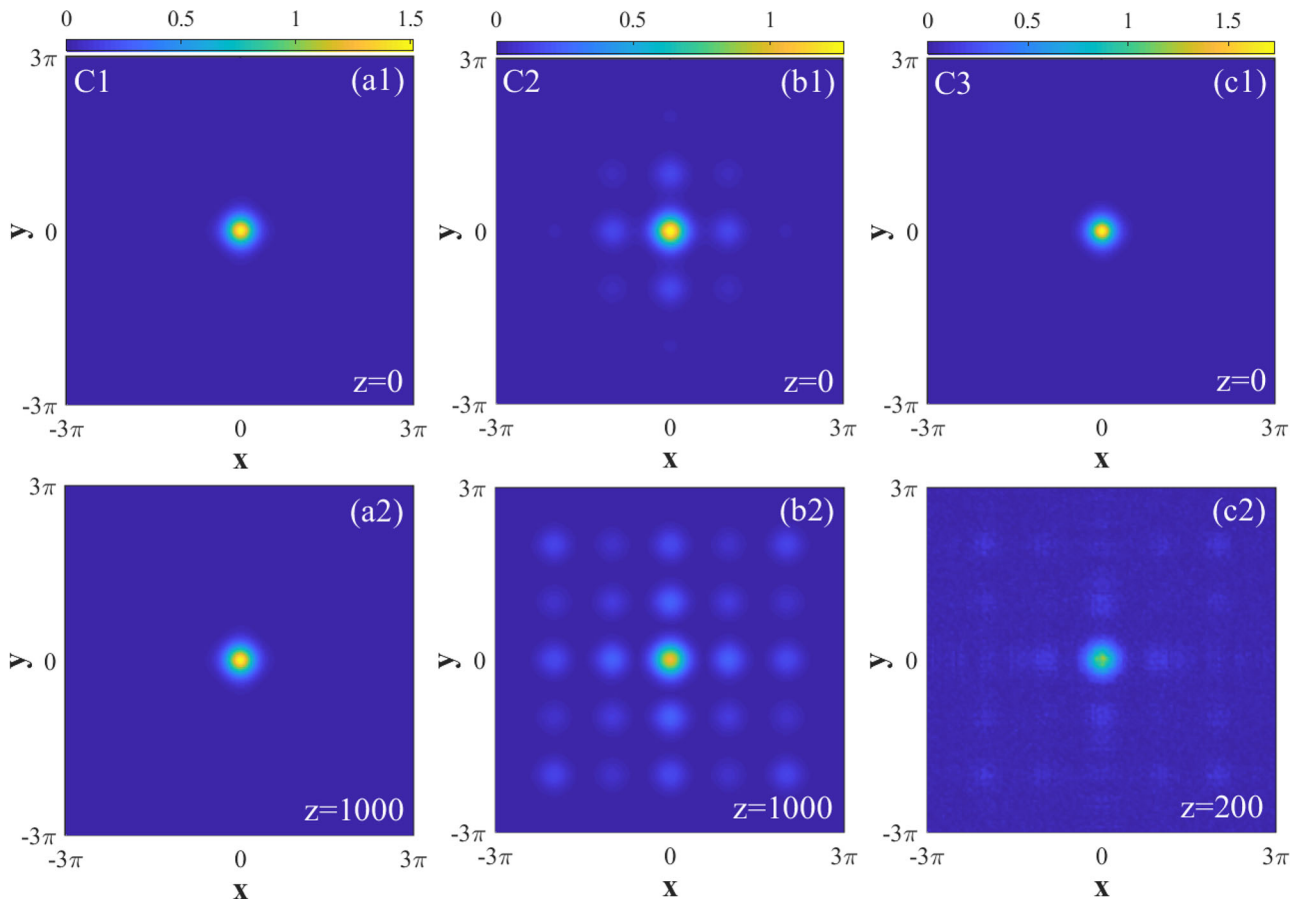


Fig. 8 | Perturbed propagations of 2D fundamental solitons. The perturbed propagation of 2D fundamental solitons in the framework of Eq. (1) with depth $V_0 = 6$ of potential (2): **a1–a2**: the stable propagation with $b = -2.8$, which

corresponds to label C1 in Fig. 5a; **b1–b2**: the unstable propagation with $b = -3.15$, which corresponds to label C2 in Fig. 5a; **c1–c2**: the unstable propagation with $b = -2.3$.

As discussed in the Introduction, the crucially important issues are the ability of the model to produce stable narrow (pixel-like) solitons. As concerns the stability, perturbed solitons solution are introduced in the usual form,

$$E(x, y, z) = [U(x, y) + p(x, y)e^{\lambda z} + q^*(x, y)e^{\lambda^* z}]e^{ibz}, \quad (8)$$

where $p(x, y)$ and $q(x, y)$ are components of the eigenmode of small perturbations with a stability eigenvalue λ , the instability taking place if there is, at least, a single eigenvalue with $\text{Re}(\lambda) > 0$, and the asterisk (*) stands for the complex conjugate. In the 1D case, the perturbed solution is sought for as

$$E(x, z) = [U(x) + p(x)e^{\lambda z} + q^*(x)e^{\lambda^* z}]e^{ibz}. \quad (9)$$

The substitution of the perturbed solution (8) into Eq. (1) and linearization with respect to the small perturbations leads to the eigenvalue problem for λ , represented by the following system of coupled equations:

$$\begin{aligned} i\lambda p &= -\frac{1}{2}\nabla^2 p + (b + V)p + gU(2U^*p + Uq) \\ &\quad + \xi U^2 U^*(3U^*p + 2Uq), \\ i\lambda q &= +\frac{1}{2}\nabla^2 q - (b + V)q - gU^*(2Uq + U^*p) \\ &\quad - \xi(U^*)^2 U(3Uq + 2U^*p). \end{aligned} \quad (10)$$

Stationary solutions are found below by means of the squared-operator method⁷⁴, then the eigenvalues of instability growth rate are calculated by the Fourier collocation method⁷⁵, and the commonly known finite-

difference marching scheme is employed to simulate the perturbed propagation of the solitons.

Estimates of the stabilization of the Townes solitons (TSs) by the lattice potential

As mentioned above, the simplest stability condition is provided by the VK criterion. In terms of definiton (4), it takes the form of

$$dP_{2D,1D}/db > 0. \quad (11)$$

Note that the solitons are unstable not only in the case of $dP_{2D,1D}/db < 0$, but also in the case of the Townes solitons (TSs) *viz.*, the 1D and 2D ones in the free space with the quintic or cubic self-focusing, respectively, which form degenerate families, whose integral power (norm) does not depend on the propagation constant, b , i.e., $dP_{2D,1D}/db = 0$ ^{26,65,76}. In particular, the family of the TS solutions of the 1D version of Eq. (5), with $g = 0$ and $\xi = 1$, is (for all positive values of b)

$$U_{\text{TS}}(x; b) = \frac{(3b)^{1/4}}{\sqrt{\cosh(2\sqrt{2b}x)}}. \quad (12)$$

The integral power of this solution indeed does not depend on b : $(P_{1D})_{g=0} = \sqrt{3}/2(\pi/2)$. The initial development of the TS instability is slow (of the power-law type, rather than exponential²⁶), as it is formally accounted for by vanishing instability growth rates. Therefore, it was possible to experimentally observe weakly unstable 2D TSs in a binary BEC under perturbation-free conditions⁷⁷.

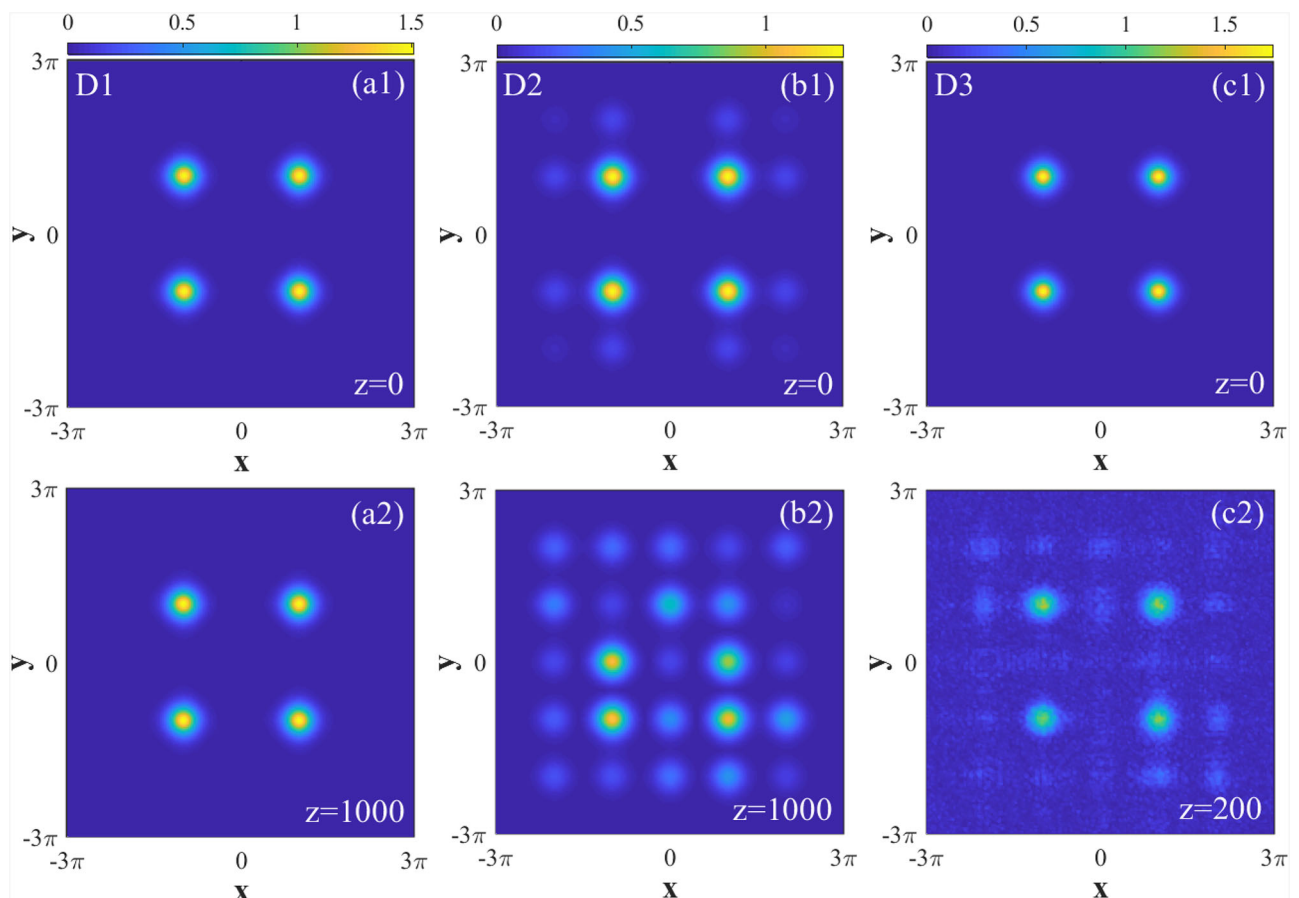


Fig. 9 | Perturbed propagations of 2D quadrupole solitons. The perturbed propagation of 2D quadrupole solitons in the framework of Eq. (1) with depth $V_0 = 6$ of potential (2): **a1–a2**: the stable propagation for $b = -2.8$, which corresponds to label

D1 in Fig. 5b; **b1–b2**: the unstable propagation with $b = -3.15$, which corresponds to label D2 in Fig. 5b; **c1–c2**: the unstable propagation with $b = -2.3$.

The VK criterion makes it possible to predict the stabilization of the TSs by the weak lattice potential [presented by the small coefficient $V_0 \ll 1$ in Eq. (3)] in the limit cases of very broad and very narrow TSs. In the former case, which corresponds to $b \ll 1$ in Eq. (12), a perturbed solution of the 1D version of Eq. (5) with $g = 0$ is looked for as

$$U(x) = U_{\text{TS}}(x; b) + \delta U_{b \ll 1}(x),$$

with correction $\delta U_{b \ll 1}(x)$ determined by the linearized equation:

$$\begin{aligned} -\beta \delta U_{b \ll 1} + \frac{1}{2} \frac{d^2}{dx^2} \delta U_{b \ll 1} - 5U_{\text{TS}}^4(x; \beta) \delta U_{b \ll 1} \\ = V_0 \sin^2 x \cdot U_{\text{TS}}(x; \beta), \end{aligned} \quad (13)$$

with $\beta \equiv b + V_0/2$. It is easy to see that, in the limit of $\beta \ll 1$, an approximate solution to Eq. (13) is

$$\delta U_{b \ll 1}(x; \beta) \approx \frac{V_0}{4} \cos(2x) \cdot U_{\text{TS}}(x; \beta). \quad (14)$$

The respective correction to the integral power P_{1D} is

$$\begin{aligned} \delta P_{b \ll 1}(\beta) &\approx 2 \int_{-\infty}^{+\infty} U_{\text{TS}}(x; b) \delta U_{b \ll 1} dx \\ &= \sqrt{\frac{3}{2}} \frac{\pi}{4} V_0 \operatorname{sech} \left(\frac{\pi}{2\sqrt{2\beta}} \right). \end{aligned} \quad (15)$$

Obviously, this expression produces $d\delta P_{b \ll 1}/db \equiv d\delta P_{b \ll 1}/d\beta > 0$, hence the VK criterion (11) holds for the broad TSs perturbed by the lattice potential, clearly suggesting the stabilization.

In the opposite limit of narrow TSs, which corresponds to $b \gg 1$ in Eq. (12), it is sufficient to expand potential (3) around the potential's minimum, $x = 0$, which replaces the 1D version of Eq. (5) with $g = 0$ by the following equation:

$$-bU = -\frac{1}{2} \frac{d^2 U}{dx^2} + V_0 x^2 U - U^5. \quad (16)$$

A simple analysis demonstrates that, in the case of large b , the respective correction to the TS solution (12), produced by the perturbation term $V_0 x^2 U$ in Eq. (16), is

$$\begin{aligned} \delta U_{b \gg 1}(x; b) &\approx \frac{3^{1/4}}{4} \frac{V_0 b^{-3/4} x^2}{\sqrt{\cosh(2\sqrt{2b}x)}} \\ &\times [1 - 2\sqrt{2b}x \tanh(2\sqrt{2b}x)], \end{aligned} \quad (17)$$

cf. Eq. (14). The respective correction to the integral power is

$$\delta P_{b \gg 1} \approx -\frac{\sqrt{3}\pi^3 V_0}{128\sqrt{2b}^2} \quad (18)$$

[cf. Eq. (15)], which also satisfies the VK criterion (11). The fact that the TS family perturbed by the lattice potential may be stable in the limits of the broad and narrow solitons suggests that the entire family may be stable. The

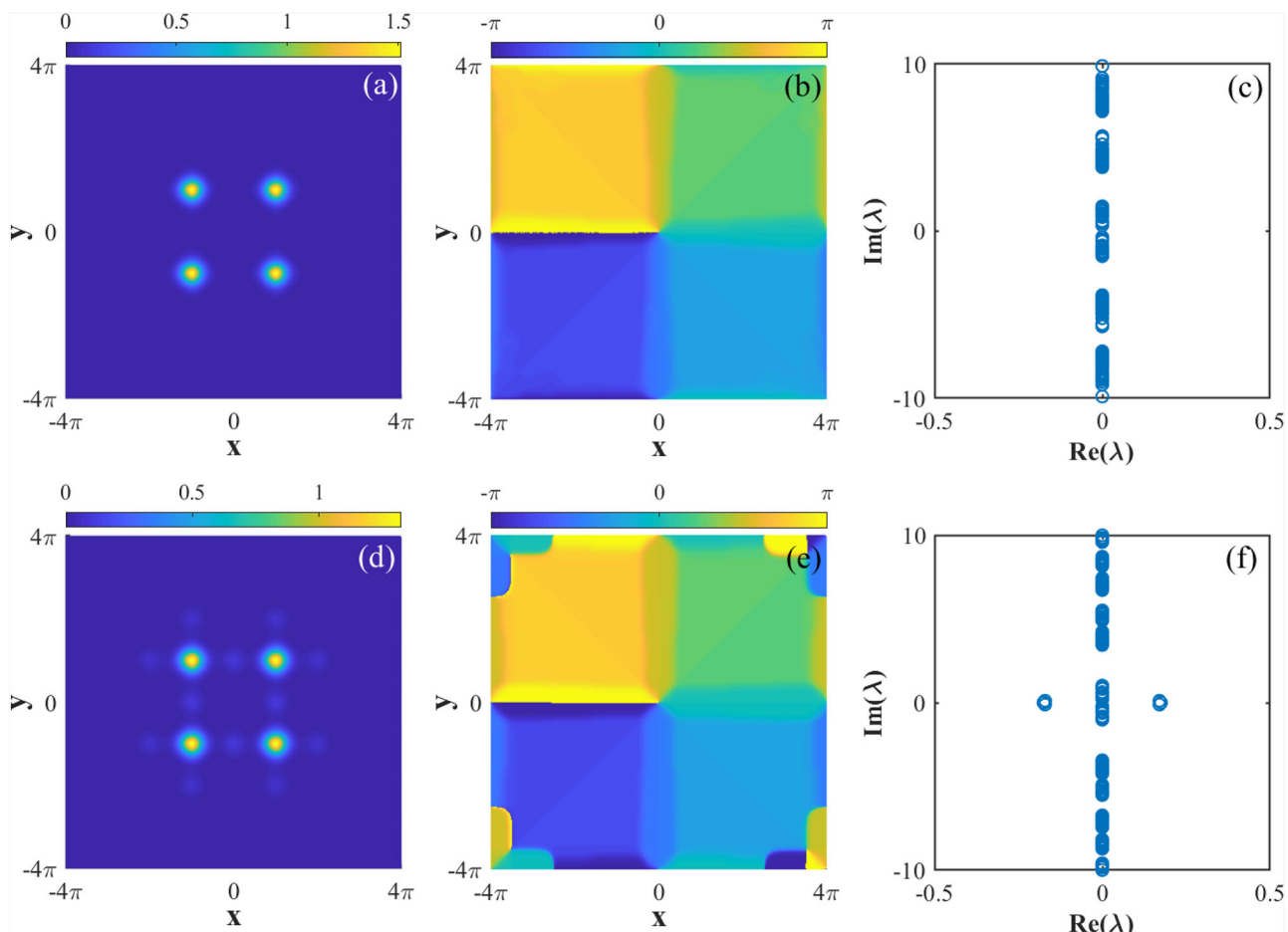


Fig. 10 | Contours, phases and eigenvalues of linear stability analysis for vortex solitons. Contours, phases, and (in)stability eigenvalues λ for stable and unstable vortex solitons with $b = -2.8$ in (a–c), and $b = -3.1$ in (d–f), respectively.

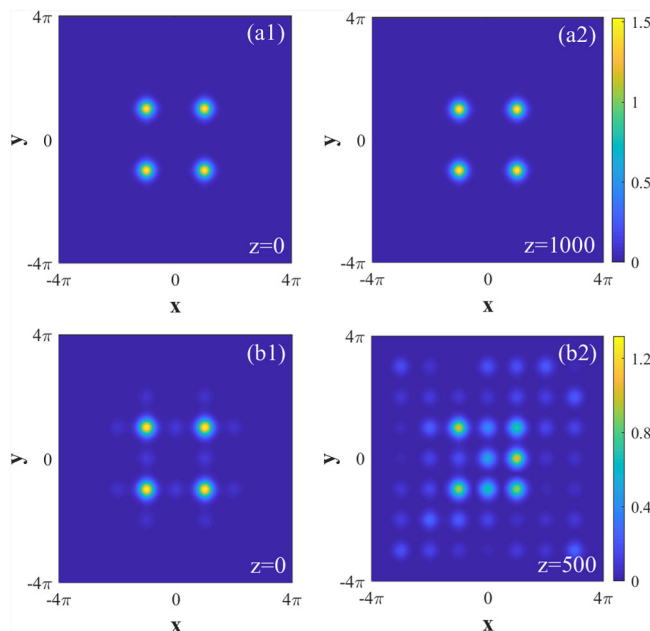


Fig. 11 | Perturbed propagations of vortex solitons. The perturbed propagation of vortex solitons in the framework of Eq. (1) with depth $V_0 = 6$ of potential (2): **a1–a2**: the stable propagation of the vortex soliton at $b = -2.8$; **b1–b2**: the unstable propagation of the vortex soliton at $b = -3.1$.

full numerical analysis confirms that, indeed, the family of 1D fundamental solitons is almost entirely stable; see Fig. 1c–f.

Data availability

The data supporting the results of this paper are available from the corresponding author upon reasonable request.

Received: 12 July 2025; Accepted: 6 October 2025;

Published online: 18 November 2025

References

1. Kivshar, Y. S. & Malomed, B. A. Dynamics of solitons in nearly integrable systems. *Rev. Mod. Phys.* **61**, 763–915 (1989).
2. Kartashov, Y. V., Malomed, B. A. & Torner, L. Solitons in nonlinear lattices. *Rev. Mod. Phys.* **83**, 247–305 (2011).
3. Konotop, V. V., Yang, J. & Zezyulin, D. A. Nonlinear waves in \mathcal{PT} -symmetric systems. *Rev. Mod. Phys.* **88**, 035002 (2016).
4. Malomed, B. A., Mihalache, D., Wise, F. & Torner, L. Spatiotemporal optical solitons. *J. Opt. B* **7**, R53–R72 (2005).
5. Leblond, H. & Mihalache, D. Models of few optical cycle solitons beyond the slowly varying envelope approximation. *Phys. Rep.* **523**, 61–126 (2013).
6. Kartashov, Y. V., Astrakharchik, G. E., Malomed, B. A. & Torner, L. Frontiers in multidimensional self-trapping of nonlinear fields and matter. *Nat. Rev. Phys.* **1**, 185–197 (2019).
7. Mihalache, D. Localized structures in optical media and Bose–Einstein condensates: an overview of recent theoretical and experimental results. *Rom. Rep. Phys.* **76**, 402 (2024).

8. Dauxois, T. & Peyrard, M. *Physics of solitons* (Cambridge University Press, 2006).
9. Mihalache, D. et al. Stable spatiotemporal solitons in Bessel optical lattices. *Phys. Rev. Lett.* **95**, 023902 (2005).
10. Mihalache, D. et al. Stable vortex tori in the three-dimensional cubic-quintic Ginzburg-Landau equation. *Phys. Rev. Lett.* **97**, 073904 (2006).
11. Zhu, X., Wang, H., Zheng, L.-X., Li, H. & He, Y.-J. Gap solitons in parity-time complex periodic optical lattices with the real part of superlattices. *Opt. Lett.* **36**, 2680–2682 (2011).
12. Zeng, L. et al. Solitons in a coupled system of fractional nonlinear Schrödinger equations. *Phys. D.* **456**, 133924 (2023).
13. Zeng, L., He, J., Malomed, B. A., Chen, J. & Zhu, X. Spontaneous symmetry and antisymmetry breaking of two-component solitons in a combination of linear and nonlinear double-well potentials. *Phys. Rev. E* **110**, 064216 (2024).
14. Si, Z.-Z. et al. Deep learning for dynamic modeling and coded information storage of vector-soliton pulsations in mode-locked fiber lasers. *Laser Photonics Rev.* **18**, 2400097 (2024).
15. Ju, Z. et al. Energy disturbance-induced collision between soliton molecules and switch dynamics in fiber lasers: periodic collision, oscillation, and annihilation. *Opt. Lett.* **50**, 1321–1324 (2025).
16. Dalfovo, F., Giorgini, S., Pitaevskii, L. P. & Stringari, S. Theory of Bose-Einstein condensation in trapped gases. *Rev. Mod. Phys.* **71**, 463 (1999).
17. Anglin, J. R. & Ketterle, W. Bose-Einstein condensation of atomic gases. *Nature* **416**, 211–218 (2002).
18. Fetter, A. L. Rotating trapped Bose-Einstein condensates. *Rev. Mod. Phys.* **81**, 647–691 (2009).
19. Frantzeskakis, D. Dark solitons in atomic Bose-Einstein condensates: from theory to experiments. *J. Phys. A* **43**, 213001 (2010).
20. Kartashov, Y. V. & Zezyulin, D. A. Stable multiring and rotating solitons in two-dimensional spin-orbit-coupled Bose-Einstein condensates with a radially periodic potential. *Phys. Rev. Lett.* **122**, 123201 (2019).
21. Kartashov, Y. V. & Konotop, V. V. Stable nonlinear modes sustained by gauge fields. *Phys. Rev. Lett.* **125**, 054101 (2020).
22. Chen, J. et al. Dark gap solitons in bichromatic optical superlattices under cubic-quintic nonlinearities. *Chaos* **34**, 113131 (2024).
23. Shah, S. A. A. et al. Qualitative analysis and new variety of solitons profiles for the (1+1)-dimensional modified equal width equation. *Chaos, Solitons Fractals* **187**, 115353 (2024).
24. Zeng, L., Mihalache, D., Zhu, X. & He, J. M-shaped solitons in cubic nonlinear media with a composite linear potential. *Nonlinear Dyn.* **112**, 3811–3822 (2024).
25. Fang, Y. et al. Deep neural network for modeling soliton dynamics in the mode-locked laser. *Opt. Lett.* **48**, 779–782 (2023).
26. Bergé, L. Wave collapse in physics: principles and applications to light and plasma waves. *Phys. Rep.* **303**, 259–370 (1998).
27. Kuznetsov, E. & Dias, F. Bifurcations of solitons and their stability. *Phys. Rep.* **507**, 43–105 (2011).
28. Fibich, G. *The Nonlinear Schrödinger Equation: Singular Solutions and Optical Collapse* (Springer, 2015).
29. Malomed, B. A. *Multidimensional solitons* (AIP Publishing LLC, 2022).
30. Baizakov, B. B., Malomed, B. A. & Salerno, M. Multidimensional solitons in periodic potentials. *Europhys. Lett.* **63**, 642 (2003).
31. Yang, J. & Musslimani, Z. H. Fundamental and vortex solitons in a two-dimensional optical lattice. *Opt. Lett.* **28**, 2094–2096 (2003).
32. Zeng, L. et al. Robust dynamics of soliton pairs and clusters in the nonlinear Schrödinger equation with linear potentials. *Nonlinear Dyn.* **111**, 21895–21902 (2023).
33. Zeng, L., Wang, T., Belić, M. R., Mihalache, D. & Zhu, X. Higher-order vortex solitons in Kerr nonlinear media with a flat-bottom potential. *Nonlinear Dyn.* **112**, 22283–22293 (2024).
34. Wang, P. et al. Localization and delocalization of light in photonic moiré lattices. *Nature* **577**, 42–46 (2020).
35. Fu, Q. et al. Optical soliton formation controlled by angle twisting in photonic moiré lattices. *Nat. Photonics* **14**, 663–668 (2020).
36. Kartashov, Y. V., Ye, F., Konotop, V. V. & Torner, L. Multifrequency solitons in commensurate-incommensurate photonic moiré lattices. *Phys. Rev. Lett.* **127**, 163902 (2021).
37. Kartashov, Y. V., Vysloukh, V. A. & Torner, L. Propagation of solitons in thermal media with periodic nonlinearity. *Opt. Lett.* **33**, 1774–1776 (2008).
38. Kartashov, Y. V., Malomed, B. A., Vysloukh, V. A. & Torner, L. Two-dimensional solitons in nonlinear lattices. *Opt. Lett.* **34**, 770–772 (2009).
39. Abdullaev, F. K., Kartashov, Y. V., Konotop, V. V. & Zezyulin, D. A. Solitons in PT-symmetric nonlinear lattices. *Phys. Rev. A* **83**, 041805(R) (2011).
40. Shi, J., Zeng, L. & Chen, J. Two-dimensional localized modes in saturable quintic nonlinear lattices. *Nonlinear Dyn.* **111**, 13415–13424 (2023).
41. Zeng, L., Malomed, B. A., Mihalache, D., Li, J. & Zhu, X. Solitons in composite linear–nonlinear moiré lattices. *Opt. Lett.* **49**, 6944–6947 (2024).
42. Neshev, D., Ostrovskaya, E., Kivshar, Y. & Krolikowski, W. Spatial solitons in optically induced gratings. *Opt. Lett.* **28**, 710–712 (2003).
43. Kevrekidis, P., Susanto, H. & Chen, Z. High-order-mode soliton structures in two-dimensional lattices with defocusing nonlinearity. *Phys. Rev. E* **74**, 066606 (2006).
44. Dror, N. & Malomed, B. A. Stability of two-dimensional gap solitons in periodic potentials: beyond the fundamental modes. *Phys. Rev. E* **87**, 063203 (2013).
45. Wang, H. & Christodoulides, D. N. Two dimensional gap solitons in self-defocusing media with PT-symmetric superlattice. *Commun. Nonlinear Sci. Numer. Simul.* **38**, 130–139 (2016).
46. Zhu, X., Belić, M. R., Mihalache, D., Cao, D. & Zeng, L. Centrosymmetric multipole solitons with fractional-order diffraction in two-dimensional parity-time-symmetric optical lattices. *Phys. D.* **470**, 134379 (2024).
47. Zeng, L. et al. Multiple-peak and multiple-ring solitons in the nonlinear Schrödinger equation with inhomogeneous self-defocusing nonlinearity. *Nonlinear Dyn.* **111**, 5671–5680 (2023).
48. Dong, L., Kartashov, Y. V., Torner, L. & Ferrando, A. Vortex solitons in twisted circular waveguide arrays. *Phys. Rev. Lett.* **129**, 123903 (2022).
49. Johansson, M. Breathing discrete nonlinear Schrödinger vortices. *Wave Motion* **131**, 103393 (2024).
50. Lobanov, V. E., Kartashov, Y. V. & Konotop, V. V. Fundamental, multipole, and half-vortex gap solitons in spin-orbit coupled Bose-Einstein condensates. *Phys. Rev. Lett.* **112**, 180403 (2014).
51. Brambilla, M., Lugiato, L., Prati, F., Spinelli, L. & Firth, W. Spatial soliton pixels in semiconductor devices. *Phys. Rev. Lett.* **79**, 2042–2045 (1997).
52. Egorov, O., Skryabin, D. V., Yulin, A. & Lederer, F. Bright cavity polariton solitons. *Phys. Rev. Lett.* **102**, 153904 (2009).
53. Quiroga-Teixeiro, M. & Michinel, H. Stable azimuthal stationary state in quintic nonlinear optical media. *J. Opt. Soc. Am. B* **14**, 2004–2009 (1997).
54. Pego, R. L. & Warchall, H. A. Spectrally stable encapsulated vortices for nonlinear Schrödinger equations. *J. Nonlinear Sci.* **12**, 347–394 (2002).
55. Feijoo, D., Zezyulin, D. A. & Konotop, V. V. Two-dimensional solitons in conservative and parity-time-symmetric triple-core waveguides with cubic-quintic nonlinearity. *Phys. Rev. E* **92**, 062909 (2015).
56. Zeng, L., Belić, M. R., Mihalache, D. & Zhu, X. Elliptical and rectangular solitons in media with competing cubic-quintic nonlinearities. *Chaos, Solitons Fractals* **181**, 114645 (2024).
57. Mihalache, D. et al. Stable spinning optical solitons in three dimensions. *Phys. Rev. Lett.* **88**, 073902 (2002).

58. Burlak, G. & Malomed, B. A. Interactions of three-dimensional solitons in the cubic-quintic model. *Chaos* **28**, 063121 (2018).
59. Quiroga-Texeiro, M., Berntson, A. & Michinel, H. Internal dynamics of nonlinear beams in their ground states: short-and long-lived excitation. *J. Opt. Soc. Am. B* **16**, 1697–1704 (1999).
60. Reyna, A. S., Jorge, K. C. & de Araújo, C. B. Two-dimensional solitons in a quintic-septimal medium. *Phys. Rev. A* **90**, 063835 (2014).
61. Reyna, A. S. & de Araújo, C. B. Spatial phase modulation due to quintic and septic nonlinearities in metal colloids. *Opt. Express* **22**, 22456–22469 (2014).
62. Reyna, A. S. & de Araújo, C. B. High-order optical nonlinearities in plasmonic nanocomposites—a review. *Adv. Opt. Photonics* **9**, 720–774 (2017).
63. Triki, H., Porsezian, K., Dinda, P. T. & Grelu, P. Dark spatial solitary waves in a cubic-quintic-septimal nonlinear medium. *Phys. Rev. A* **95**, 023837 (2017).
64. Triki, H. & Kruglov, V. I. Chirped periodic and localized waves in a weakly nonlocal media with cubic-quintic nonlinearity. *Chaos, Solitons Fractals* **153**, 111496 (2021).
65. Abdullaev, F. K. & Salerno, M. Gap-townes solitons and localized excitations in low-dimensional Bose-Einstein condensates in optical lattices. *Phys. Rev. A* **72**, 033617 (2005).
66. Vakhitov, N. G. & Kolokolov, A. A. Stationary solutions of the wave equation in the medium with nonlinearity saturation. *Radiophys. Quantum Electron.* **16**, 783–789 (1973).
67. Louis, P. J., Ostrovskaya, E. A., Savage, C. M. & Kivshar, Y. S. Bose-Einstein condensates in optical lattices: band-gap structure and solitons. *Phys. Rev. A* **67**, 013602 (2003).
68. Efremidis, N. K. & Christodoulides, D. N. Lattice solitons in Bose-Einstein condensates. *Phys. Rev. A* **67**, 063608 (2003).
69. Efremidis, N. K. et al. Two-dimensional optical lattice solitons. *Phys. Rev. Lett.* **91**, 213906 (2003).
70. Peleg, O. et al. Conical diffraction and gap solitons in honeycomb photonic lattices. *Phys. Rev. Lett.* **98**, 103901 (2007).
71. Wang, X. et al. Observation of two-dimensional surface solitons. *Phys. Rev. Lett.* **98**, 123903 (2007).
72. Hukriede, J., Runde, D. & Kip, D. Fabrication and application of holographic Bragg gratings in lithium niobate channel waveguides. *J. Phys. D* **36**, R1 (2003).
73. Göksel, İ., Antar, N. & Bakırtaş, İ. Solitons of (1+1) D cubic-quintic nonlinear Schrödinger equation with \mathcal{PT} -symmetric potentials. *Opt. Commun.* **354**, 277–285 (2015).
74. Yang, J. & Lakoba, T. I. Universally-convergent squared-operator iteration methods for solitary waves in general nonlinear wave equations. *Stud. Appl. Math.* **118**, 153–197 (2007).
75. Yang, J. *Nonlinear Waves in Integrable and Nonintegrable Systems* (SIAM, 2010).
76. Chiao, R. Y., Garmire, E. & Townes, C. H. Self-trapping of optical beams. *Phys. Rev. Lett.* **13**, 479–482 (1964).
77. Bakkali-Hassani, B. et al. Realization of a townes soliton in a two-component planar Bose gas. *Phys. Rev. Lett.* **127**, 023603 (2021).

Acknowledgements

This work is supported by National Natural Science Foundation of China (62205224, 11774068), Guangdong Basic and Applied Basic Research Foundation (2023A1515010865), Guangzhou Science and Technology Plan Project (2025A04J4068), and Start-up Foundation for Talents of Guangzhou Jiaotong University (K42022076, K42022095).

Author contributions

L.Z. has contributed to the idea, the numerical simulations, and written the first draft of the paper. B.A.M. and D.M. carried out the theoretical analysis, discussed the results and revised the manuscript. X.Z. has contributed to the idea, the numerical simulations and revised the manuscript.

Competing interests

The authors declare no competing interests.

Additional information

Supplementary information The online version contains supplementary material available at <https://doi.org/10.1038/s42005-025-02355-z>.

Correspondence and requests for materials should be addressed to Xing Zhu.

Peer review information *Communications Physics* thanks Rama Gupta, Yi-Xiang Chen and the other, anonymous, reviewer(s) for their contribution to the peer review of this work. A peer review file is available.

Reprints and permissions information is available at <http://www.nature.com/reprints>

Publisher's note Springer Nature remains neutral with regard to jurisdictional claims in published maps and institutional affiliations.

Open Access This article is licensed under a Creative Commons Attribution-NonCommercial-NoDerivatives 4.0 International License, which permits any non-commercial use, sharing, distribution and reproduction in any medium or format, as long as you give appropriate credit to the original author(s) and the source, provide a link to the Creative Commons licence, and indicate if you modified the licensed material. You do not have permission under this licence to share adapted material derived from this article or parts of it. The images or other third party material in this article are included in the article's Creative Commons licence, unless indicated otherwise in a credit line to the material. If material is not included in the article's Creative Commons licence and your intended use is not permitted by statutory regulation or exceeds the permitted use, you will need to obtain permission directly from the copyright holder. To view a copy of this licence, visit <http://creativecommons.org/licenses/by-nc-nd/4.0/>.

© The Author(s) 2025